Proceedings World Geothermal Congress 2015
Melbourne, Australia, 19-25 April 2015

Flow Lognormality and Spatial Correlation in Crustal Reservoirs: III -- Natural Permeability Enhancement via Biot Fluid-Rock Coupling At All Scales

Justin Pogacnik, Peter Leary, Peter Malin, Peter Geiser, John Rugis & Brice Valles

Institute of Earth Science & Engineering, University of Auckland, New Zealand

p.leary@auckland.ac.nz

Keywords: EGS, reservoir flow, fracture stimulation, permeability stimulation, spatial correlation, lognormality

ABSTRACT

Fluid-rock mechanical interaction is important to crustal processes, yet little is known of the *in situ* physics. Typically fluid-rock interaction is expressed by folding fluid pressure into Hooke's Law, through the concept of effective stress. As conceived, the effective stress relationship treats rock as a continuum with pore pressure smoothly distributed within the granular matrix without consideration of microscale rock evolution. Recent advances have revealed the inhomogeneity of crustal fluid-rock interaction over a wide range of length scales. Consideration of this inhomogeneity of rock properties leads to a natural permeability enhancement relationship that respects microscale evolution of the rock fabric. Our computation suggests that order of magnitude permeability stimulation in the vicinity of wellbores is a plausible target. An immediate application of such *in situ* permeability enhancement is to increase the 'effective radius' of the wellbore. Larger wellbore 'effective radii' increase heat recovery efficiency by reducing thermal gradient heat loss near EGS wellbores.

1. INTRODUCTION

The concept of heat extraction from generic low-permeability hot crustal rock at drillable depths has long been based on the hydrocarbon industry 'continuum-discontinuum' view of fluid-rock interaction in crustal rock. In this view, fluids are largely a passive partner in the mechanics of rock deformation, filling isolated voids, moving between connected voids, and lubricating rough frictional surfaces by exerting zero-rigidity normal stress. The passive mechanical role of *in situ* fluids as a scalar component of stress appears in the standard generalization of Hooke's Law,

$$\sigma_{ij} - p\delta_{ij} = c_{ijkm}\, e_{km}, \qquad (1)$$

in which the stress tensor σ_{ij} modified by the scalar pressure field p is linearly related to the strain tensor e_{km} through a set of elastic constants c_{ijkm}. Eq (1) was first given for soil mechanics by Terzaghi (1925), adopted for unconsolidated rock by Biot (1941), and applied to large-scale geological thrust faulting by Hubbert & Rubey (1959).

In many if not most reservoir applications, (1) is interpreted for fluids as passively seeping through 'effectively-uniform' continuum of pores and pore connectivity except where the continuum is fractured into mechanically discontinuous sections (Theis 1935; Muskat 1937; Biot 1941; Horner 1951; Grindley 1965; Bodvarsson 1969; Jaeger & Cook 1979; Horne 1995; Hanano 2000; Mavko, Mukerji & Dvorkin 2003; Tester et al 2006; Juliusson 2012). This view strengthened during the 1950s evolution of wellbore hydraulic fracturing to increase oil recovery (Hubbert & Willis 1957; Howard & Fast 1970), and was comprehensively adopted for geothermal application to low-permeability 'hot dry rock' formations (e.g., Gringarten & Witherspoon 1973; Gringarten, Witherspoon & Ohnishi 1975; Wunder & Murphy 1978; Pruess & Narasimhan 1985; Armstead & Tester 1987; Elsworth 1989, 1990; Heuer, Kupper & Windelberg 1991; Horne 1995; Tester et al. 2006; Sutter et al. 2011).

Figure 1 from Tester et al (2006) abstracts the standard view of the mechanical role of fluids in geothermal reservoirs: seeping through a quasi-uniform matrix continuum and moving more rapidly along km-scale crustal volumes populated by well-connected planar mechanical discontinuities induced in crustal volumes by hydrofracturing. Four decades of attempts to apply Figure 1 concepts of wellbore hydraulic fracture stimulation to 1km-scale low-permeability hot dry rock volumes have, however, proved largely unable to achieve significant flow into the surrounding rock, let alone yield high-flow connectivity between well pairs at commercially relevant offsets >> 100m. The following texts (Tester et al. 2006 unless noted) summarize the mismatch between the continuum/discontinuum concepts and *in situ* reality:

- Fenton Hill, USA, 1970s – *Although the reservoir had the potential of producing 1 million m^2 of heat-transfer surface, based on the fluid volume pumped, the fracture pattern that was observed did not match that predicted by early modelling.*
- Rosemanowes, UK, 1980s – (i) *The fractures created by hydraulic stimulation…..are not formed through tension, as in the hydraulic fracturing used in oil and gas wells. Instead, they are created by shearing on pre-existing joint sets.* (ii) *…..the fractures may not grow exactly as predicted;* (iii) *Probably the most important single lesson from this experiment is that hydro-fracturing and artificial fractures are almost irrelevant. The natural fracture system dominates everything.*
- Soultz, France, 1990s-2000s – (i) *Natural fractures and the natural connectivity of these fractures seem to dominate the enhanced reservoir system.* (ii) *Natural fractures can be stimulated, but there seems to be little data to support the creation of a totally artificial reservoir when no natural fractures are present.*
- Paralana, Australia, 2011 – *The fracture array cloud measured by the array indicated that it extended 300m by 200m and was approximately 130m thick* (Reid et al. 2011).

- Newberry, USA, 2013 – Disseminated seismic activity fracture stimulation in 1.5km x 0.7km x1km crustal volume with no evidence of fracture-dominated flow structure by which to target production well drilling for well-to-well flow (Petty 2013).

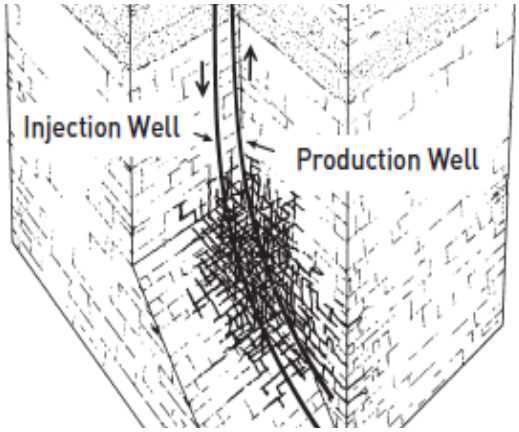

Fig 1 – Illustration of EGS principle of operation from Tester et al (2006): Crustal heat is to be extracted by thermal conduction from rock volumes by fluid flowing along planar fracture structures created in situ by hydrofracturing.

While effective media approximations based on spatial averaging is deeply entrenched in treatments of crustal reservoir flow (Theis 1935; Biot 1941; Horner 1951; Freeze 1975; Earlougher 1977; Horne 1995; Kitanidis 1997; Jensen et al. 1997; Mavko, Mukerji & Dvorkin 2003), a great deal of geological and geophysical evidence argues that rock is not an effectively elastic continuum that supports uniform seepage flow unless broken at quasi-planar discontinuities. A large number of well-known crustal processes have been described and/or understood in terms of heterogeneous distributions of elastic discontinuities on all scales from mm (grains) to km (reservoirs, mountains, upper crustal thickness), with or without regard to complex mechanical interactions with *in situ* fluids:

- Fractal scaling of earthquake dimension (Gutenberg & Richter 1956; Hanks & Kanamori 1979; King 1983; Hirata 1989);
- Earthquake clustering (Kagan & Knopoff 1980; Hirata, Satoh & Ito 1987);
- Earthquake triggering by small reservoir surface loads (Simpson & Negmatullaev 1980; Simpson, Leith & Scholz 1988);
- Inability to predict earthquakes (Geller et al. 1997; Leary 1997);
- Seismic coda wave scattering (Leary & Abercrombie 1994a,b; Leary 2002a,b);
- Scale-dependent crustal permeability (Brace 1980; Clauser 1992; Neuman1994,5; Winter &Tartakovsky 2001), dispersivity (Gelhar 1986; Gelhar, Welty & Rehfeldt 1992), Schulze-Makuck & Cherhauer 1995, and rock strength (Bandis 1980; Dunnicliff 1993; Baghbanan & Jing 2008; Pusch, Weston & Knutsson 2014);
- Mountain building and erosion (Davis, Suppe & Dahlen 1983; Dahlen, Suppe & Davis 1984s; Dahlen 1990; Molnar, Anderson & Anderson 2007);
- Mass solution transfer of large crustal volumes (Geiser & Sansone 1980; Engelder & Geiser 1981).

In recent years a number of widely attested rock-fluid interaction empirics spanning the microscopic grain-scale ~ mm to the megascopic reservoir-scale ~ km have shown that rock-fluid mechanical interactions to be far more spatially complex than commonly perceived. The attested rock-fluid inhomogeneity is rooted in the grain-scale properties of rock and indicates that *in situ* fluid pressure can vary in conjunction with grain-scale permeability fluctuations to interact with grain-scale rock fabric. The grain-scale-based features of *in situ* crustal rock-fluid interaction go well beyond the 'effective-medium' assumption generally associated with (1). The following sections of this paper make explicit many physical aspects of *in situ* fluid-rock interaction, embed the fluid-rock interaction in a revised expression of Biot (1941) stress equilibrium in a saturated porous medium constructed along lines of empirical evidence, and illustrate the heat-transfer response to potential EGS permeability-stimulation interventions associated with wellbores.

2. AN EMPIRICAL PERSPECTIVE ON *IN SITU* FLUID-ROCK INTERATION

The passive mechanical nature of *in situ* fluids in rock as an elastoporous continuum usually associated with the effective stress expression of (1) is belied by extensive range of empirical data recorded by well-logs, well-core sequences, and well-flow statistics. These fluid-rock interaction empirics are summarised by the following points:

- Rock granularity can be approximated as a dual population of intact grain-grain cement bonds hosting defective grain-grain cement bonds that transmit fluids (Leary 1997, 2002);
- Grain-scale cement-bond defects are randomly distributed, but the randomness is spatially correlated at scales from mm to km (fluctuation power scaling inversely with spatial frequency) and is both highly erratic and non-uniform at all spatial scales (Leary 1991, 2002);
- Spatial fluctuations in the logarithm of permeability in rock are closely associated with spatial fluctuations in porosity; grain-scale defects are percolation pathways for *in situ* fluids over all scale lengths (Leary & Al-Kindy 2002; Pogacnik, Leary & Malin 2013);
- Grain-scale defect density is a percolation-threshold 'critical state' parameter (Leary 1997, 2002);

- Median *in situ* permeability increases with physical dimension from cm to km (Gelhar, Welty & Rehfeldt 1992; Clauser 1992; Neuman 1994);
- Spatial fluctuations in *ini situ* permeability are lognormally distributed at all scale lengths (Law 1944; Ahrens 1963; Koch & Link 1971; Zikovsky & Chah 1990; Limpert, Stahel & Abbt 2001; Leary et al 2014);
- Spatial fluctuations in the logarithm of permeability in clay are closely associated with spatial fluctuations in clay void ratio (Taylor 1948; Mesri & Olson 1971; Tavernas et al 1983).

These empirics allow quantitative expression of fluid-rock interaction properties at all scale lengths that accord with the above cited qualitative evidence for *in situ* spatial heterogeneity of rock/fluid property distributions. Coupling *in situ* porosity φ in rock (void ratio $\varepsilon = \varphi/(1-\varphi)$ in clays) to *in situ* permeability κ is of particular interest *re* addressing the engineering interventions to increase *in situ* permeability. For clastic reservoir rock, sequences of well-core porosity fluctuations $\delta\varphi$ are seen to be closely correlated to fluctuations in the logarithm of well-core permeability $\delta log(\kappa)$,

$$\delta\varphi \propto \delta log(\kappa). \qquad (2)$$

Small-scale spatial fluctuation relation (2) can be integrated over large-scale well-core sequences to characterise the volumetric distribution of permeability in terms of the volumetric distribution of porosity,

$$\kappa(x,y,z) \approx \kappa_0 \, exp(\alpha(\varphi(x,y,z)-\varphi_0)), \qquad (3)$$

for median values of porosity and permeability φ_0 and κ_0 in the crustal volume, and α an empirical parameter typically >> 1.

Relationships (2)-(3) between *in situ* permeability $\kappa(x,y,z)$ and *in situ* porosity $\varphi(x,y,z)$ can be directly measured through plotting the logarithm of permeability versus porosity recorded in well-core sequences. As illustrated in Figure 2, the plots estimate integration parameter α for a well-core sequence. Two well-core data suites provide porosity-log(permeability) trends denoted by blue dots; the red line fits to the data trends return the value of parameter α for each sequence. In Figure 2, porous sands have $\alpha \sim 15 \pm 2$ (left), and fracture-intense tight gas sands have a higher value $\alpha \sim 26 \pm 7$ (right).

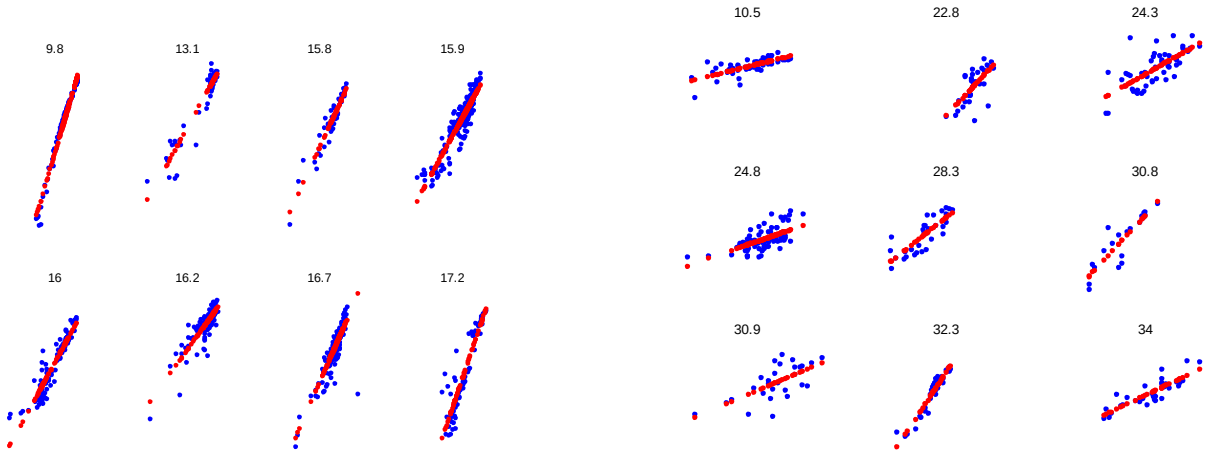

Figure 2 – Cross-plots for well-core poroperm sequences in North Sea oil reservoir (left) and South Australia tight gas-sands (right). For each poroperm sequence porosity is plotted horizontally and logarithm of permeability vertically; the mean plot trend shown in red gives the value of α in (3), $\kappa \sim \kappa 0 \, exp(\alpha(\varphi-\varphi 0))$.

The Figure 2 values for α are consistent with lognormal distributions of *in situ* flow distributions measured by well productivity. Values of α in the range 30-50 are attested throughout commercial (oil/gas/geothermal/mineral) reservoir data (e.g., Law 1944; Ahrens 1963; Koch & Link 1971; Zikovsky & Chah 1990; Limpert, Stahel & Abbt 2001; Leary et al 2014). Observed equivalents to (2)-(3) and Figure 2 are also observed in clays (Taylor 1948; Mesri & Olson 1971; Tavernas et al 1983).

The statistical systematics of well-core integration parameter α are illustrated in Figure 3, where it is shown that increasing values of α are directly equivalent to increasing degrees of lognormality and increasing values of maximum permeability. Beginning with low α values ~ 3 in the upper left corner, the permeability distributions given by (3) become increasing skewed toward small values of permeability as α increases towards ~ 50 in the lower right corner. With the increasing skewness of the distributions, the effective permeability of the distribution increases rapidly from values around unity for small α to high permeability flow structures in the 10 to 20 range for $\alpha \sim 50$. *In situ*, high productivity wells tend to be connected to high production flow systems as expected if *in situ* flow is governed by fracture-system connectivity and fracture connectivity increases with increasing porosity as noted for shale reservoirs in Paper II, Malin et al (2015); we can hence regard increased permeability in Figure 3 to be associated with increasing percolation flow pathways, which is the goal of EGS permeability stimulation.

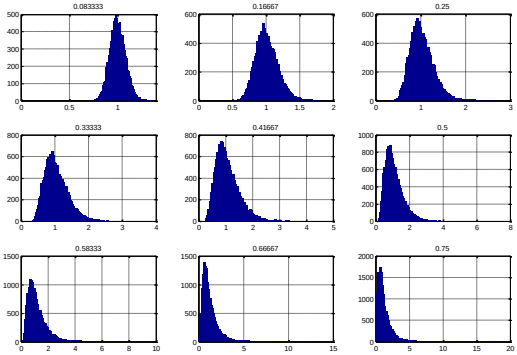

Figure 3 – Progression from normal distributions (upper left) to lognormal distributions (lower right) of in situ permeability κ(x,y,z) given by (3) as a function of empirical integration parameter α for a fixed distribution of in situ porosity φ(x,y,z). Values of α < 10 give normal-to-near-normal permeability distributions; observed values of α in range 30 < α < 60 correspond to increasingly lognormal permeability distributions observed in reservoirs everywhere.

Spatial coupling (2)-(3) and Figures 2-3 for *in situ* porosity and permeability has not been previously advanced as an aspect of fluid-rock interactions. The details of fluid-rock interaction can be heuristically understood in terms of fracture-connectivity within a population of grain-scale fractures in a unit of crustal rock. If we let n be the number of grain-scale fractures associated with porosity, $\varphi \propto n$, in a unit volume of crustal rock, we can suppose the permeability of that volume increases with grain-scale fracture number n in proportion to the factorial of the grain-scale defect density, $\kappa \propto n!$. Stirling's identity $log(n!) \sim nlog(n) - n$ reduces to expression $\delta log(n!) \propto \delta n$, thus recovering empirical relation (2) $\delta\varphi \propto \delta log(\kappa)$ in terms of *in situ* flow via percolation along grain-scale fracture-connectivity pathways at all scales.

Building on the empirical systematics of fluid-rock coupling expressed heuristically in terms of grain-scale-defect coupling at all scale lengths, we can rewrite (2) in terms of positive feedback increments of permeability as a function of porosity:

$$\delta\kappa \approx \kappa\, \delta\varphi. \tag{4}$$

Equation (4) is empirical evidence that permeability increments δκ occur most readily at rock volume sites having pre-existing permeability κ and a natural predilection in rock for defects associated with locally high porosity fluctuation δφ. This coupling points directly to a generic interaction of fluid pressure and grain-scale rock fabric in a feedback geomechanical interaction that can result in enhanced permeability. Higher permeability allows fluid pressures to abate more quickly, indicating a fluid-solid coupling energetics that encourages *in situ* permeability enhancement (4) throughout a crustal reservoir complex.

The practical aspect of permeability enhancement mechanism (4) is the detailed fluid-rock interaction that can be applied *in situ* to engineer increases in rock permeability surrounding a wellbore. For this purpose we express the Biot (1941) equations for saturated fluid-rock interaction by including heterogeneity we know exists in rock. Eqs. (5a-b) are the *x*- and *y*-components of a revised set of Biot equilibrium conditions for 2D plane-strain deformation (u,$\underline{v}$) of poroperm media in which elastic rigidity $G(\varphi)$ and Poisson's ratio $\nu(\varphi)$ vary in space as a direct function of porosity $\varphi(x,y)$:

$$G\nabla^2 u + G(1+\nu)/(1-\nu)\varepsilon_x = p_x - 2G_x(u_x/(1-\nu) + v_y) - 2Gv_x/(1-\nu)^2 - G_y(u_y + v_x) \tag{5a}$$

$$G\nabla^2 v + G(1+\nu)/(1-\nu)\varepsilon_y = p_y - 2G_y(u_x/(1-\nu) + v_y) - 2Gv_y/(1-\nu)^2 - G_x(u_y + v_x), \tag{5b}$$

where subscripts x,y denote partial derivatives ∂_x,∂_y, $\varepsilon = u_x + v_y$ is volumetric strain, and $p(x,y)$ is fluid pressure.

We know from well-log spatial fluctuation data that the right-hand side of (5) is non-negligible in relation to the left-hand side. We can thus say that (5) represents an essential corrective to the standard ('effective medium') approach to *in situ* fluid-solid coupling. Equations such as (5) can be expressed numerically in grids of sufficient density that the spatial complexity of rock can be effectively represented (e.g. Paper I, Leary et al 2015), and hence the right-hand side of (5) can adequately express the spatial distribution of energy, stress and strain in a crustal volume with attention to grain-scale complexity essential for understanding *in situ* permeability. Numerical exploration of (5) can establish the conditions for incremental changes in grain-scale fracture connectivity, and as such can be considered as a logical starting point for exploring *in situ* permeability processes.

3. PRESSURE-ENHANCEMENT OF NEAR-WELLBORE PERMEABILITY IN GEOCRITICAL POROPERM MEDIA

The *in situ* properties of rock-fluid interaction are not necessarily evident or accessible in small rock samples or at the near surface. Much more plausible means for exploring *in situ* fluid-rock interaction is at depth in the vicinity of a wellbore at depth. Accordingly we cast our numerical exploration of fluid-rock coupling in terms of a wellbore-centric section of crustal rock. Figure 4 represents the porosity distribution of a section of crustal rock 6m in diameter surrounding a 16cm wellbore. The porosity section distribution in Figure 4 is extracted from a larger porosity volume having the empirical long-range spatial correlation grain-scale fluctuations properties of *in situ* rock summarised in §2 (cf Paper II, Malin et al 2015). In particular, *in situ* spatial fluctuation data strongly attest a tendency at all scale lengths for porosity fluctuations to cluster, here indicated by higher porosity groupings in warm colors, to form natural percolation connectivity flow paths for *in situ* fluids on all scale lengths. The spatial heterogeneity

shown in figure 4 is characteristic of rock everywhere, and embodies the fluid-rock interactions that are generically overlooked in effective medium treatments of crustal rock.

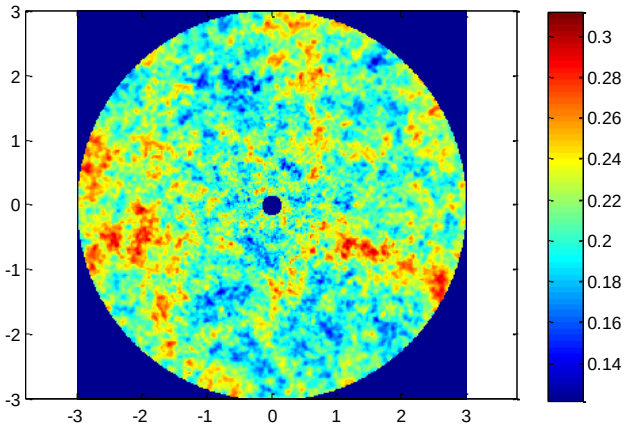

Figure 4 – 2D numerical distribution representing porosity fluctuations in crustal rock at 6m scale about a 16cm radius wellbore; the porosity slice is from a 3D numerical volume having the empirical long-range spatial correlation grain-scale fluctuations described by empirical attributes summarized in §2.

For media with spatial porosity fluctuations, as in Figure 4, and associated spatial fluctuating poroperm properties, wellbore fluids under pressure percolate into the surrounding medium via fracture-connectivity pathways. Elevated fluid pressures create spatial dislocations as a function of the porosity distribution according to Biot stress equilibrium (5). Figure 5 shows two manifestations – von Mises stress on left, principal strain on right -- of the resultant localized stresses and strains responding to fluid pressure in close congruence with the porosity fluctuations.

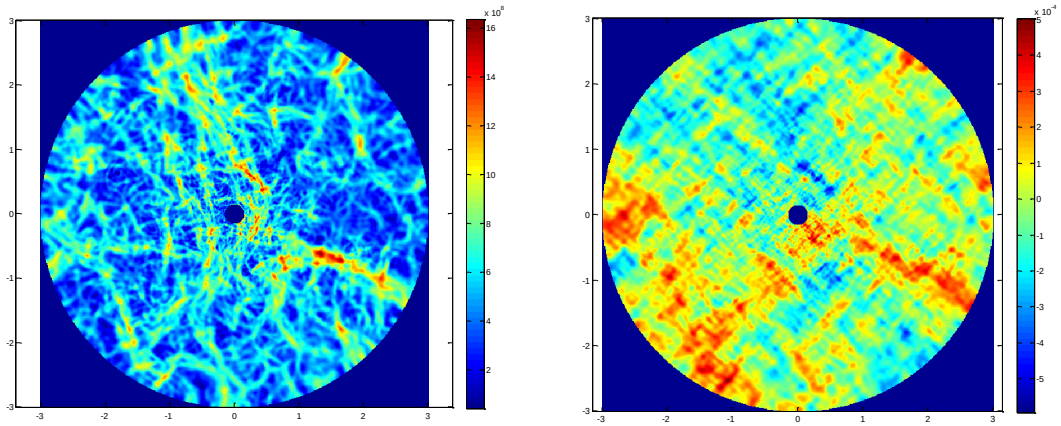

Figure 5 – Spatial distributions of von Mises stress (left) and principal strain (right) for Fig 4 poroperm medium subjected to sustained wellbore fluid pressurisation as given by Biot stress-equilibrium condition (5). Wellbore-pressure-induced stress/strain levels in poroperm media can be expected to intensify grain-scale fracture density fluctuations in proportion to the local porosity fluctuations, hence to increase the potential for local fracture-connectivity pathways to pass percolating fluids, i.e., increase local permeability. The increase in permeability can be parameterized as an increase in the spatially variable value of $\alpha(x,y)$, $\alpha \rightarrow \alpha + d\alpha$, in empirical relation (3), $\kappa \approx \kappa 0 \exp(\alpha(\varphi-\varphi 0))$.

The spatial congruence of the empirically attested porosity distribution of Figure 4 and calculated pressure-induced stresses and strains of Figure 5 indicate that the Biot link (5) is a plausible microphysical mechanism by which long-range spatial correlations arise in crustal rock everywhere. It is reasonable to expect that fluid-pressure-induced stress/strain levels in poroperm media intensify grain-scale fracture density fluctuations in rough proportion to the local porosity fluctuations. It is further reasonable to expect that increasing fracture density increases the potential for local fracture-connectivity pathways to pass percolating fluids.

Empirical relation (3) $\kappa \approx \kappa_0 \exp(\alpha(\varphi-\varphi_0))$ indicates that increased percolation flow can be expressed as increases in the value of the spatially variable parameter $\alpha(x,y)$ by which episodes of fluid pressurisation induce changes $\alpha \rightarrow \alpha + d\alpha$. Figure 5 indicates that it is possible in principle to induce higher *in situ* permeabilities through wellbore pressurisation. A sequence of incremental pressurizations of the Figure 4 wellbore-centric section leading the growth of α due to to incremental increases in induced stress and strain in Figure 4 creates a sequence of α-value distributions for the Figure 4 crustal section. The pressurization sequence is summarized in Figure 6, built on a recursive sequence of figures like Figure 5 by which numerical pressure-induced changes in fracture-connectivity parameter $\alpha \rightarrow \alpha + d\alpha$ bring a poroperm medium of low initial permeability equivalent to $\alpha \sim 4$ (magenta/blue poroperm trend) to a poroperm medium of high permeability equivalent to $\alpha \sim 33$ (red/black poroperm trend).

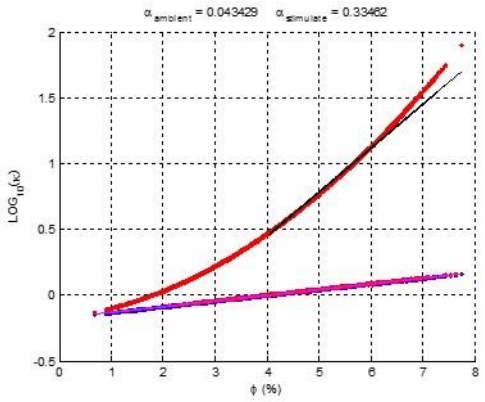

Figure 6 – Initial (blue/magenta) and final state (red/black) poroperm cross-plots for permeability stimulation sequence. Fig 2 shows a close correspondence between porosity and log(permeability) exists in situ. Initial/final model α-values are respectively 4.3 and 33.4 reflect the range of values seen in Figure 3.

4. APPLICATION OF IN SITU WELLBORE-CENTRIC PERMEABILITY ENHANCEMENT

We can assess the permeability needs of the EGS flow system by modelling advective heat transport in relation to conductive heat transport for wellbore-centric crustal sections with the poroperm properties of the Figures 3-4 crustal sections. We compute the steady-state temperature distribution according to heat energy conservation condition,

$$\nabla^2 T = \rho C/K\, \boldsymbol{\nabla}\cdot(\boldsymbol{v}T) = \rho C/K\, (T\boldsymbol{\nabla}\cdot\boldsymbol{v} + \boldsymbol{v}\cdot\boldsymbol{\nabla}T) = \rho C\kappa\mu p_0/K\, (T\boldsymbol{\nabla}\cdot\boldsymbol{\nabla}P + \boldsymbol{\nabla}P\cdot\boldsymbol{\nabla}T), \qquad (6)$$

for which the unknown temperature distribution T is solved for given/constant advective velocity field $\boldsymbol{v}$ for a specific EGS system dimension and wellbore geometry (cf. Paper I; Leary, Pogacnik & Malin 2012, 2013; Pogacnik, Leary & Malin 2013). System constants in the collective coefficient term $A \equiv \rho C\kappa\mu P_0/K$ are the density, heat capacity, viscosity of water ($\rho \sim 10^3$kg/m^3, $C \sim 4.3\ 10^3$J/kg·^{o}C, $\mu \sim 2\ 10^{-4}$Pa·s), the thermal conductivity of rock ($K \sim 3$W/m·^{o}C), the mean permeability κ [m^2] of the section and the pressure scale p_0 [Pa] normalizing system pressure $P = p/p_0$. Scaling constant $A = \rho C\kappa\mu P_0/K$ is of order unity for permeability/pressure range ~100mDarcy/100bar ($\kappa \sim 10^{-13}$m^2/$P_0 \sim 10^7$Pa) to ~10mDarcy/1Kbar ($\kappa \sim 10^{-14}$m^2/$P_0 \sim 10^8$Pa).

Figure 7 illustrates the utility of *in situ* permeability stimulation achieving larger 'effective radii' wellbores. Larger effective wellbore radii reduce thermal gradients associated with wellbore flow, hence enable more efficient heat transport. As shown in Figure 7 (left) advective heat flow via narrow gauge wellbores in a uniform poroperm κ = 10mDarcy flow medium leads to a temperature distribution with ~100^{o}C heat at radii ~10-15m and ~170^{o}C heat at 50m radii. If each wellbore is increased in effective radius by increasing permeability to 100mDarcy over a 3 meter radius, the right hand side of Figure 7 shows 150°C heat at radii ~10-15m and ~190°C heat at 50m radii. Higher advection transports heat at higher temperatures and/or lower pressures than lower advection.

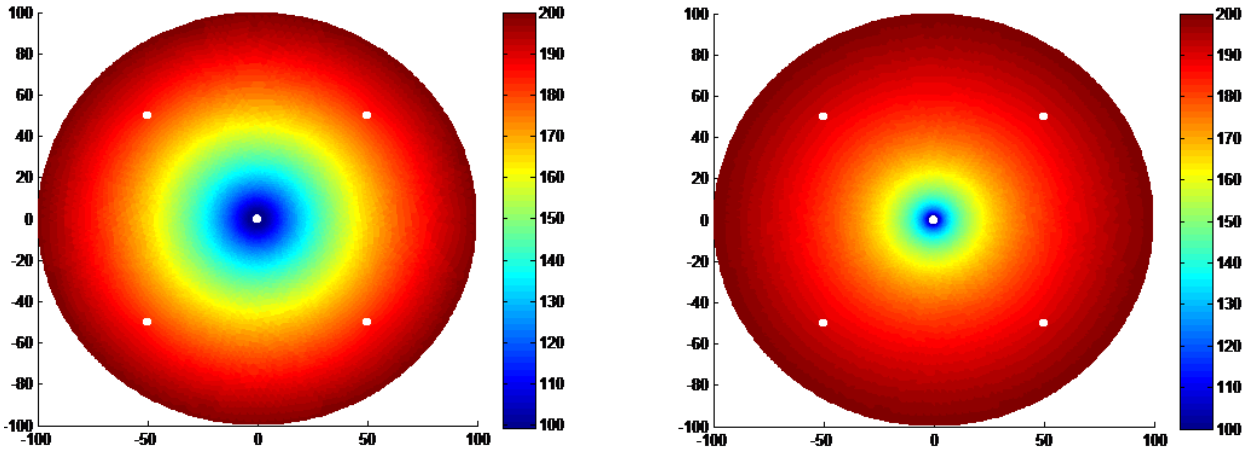

Figure 7 – Effect of wellbore-centric permeability stimulation on advective transport heat distribution in EGS section of Fig 3 scaled to 100m radius. (Left) Advective flow temperature field for uniform permeability κ = 10mDarcy for 1m wellbore radii. (Right) Advective flow temperature field in which permeability in vicinity of each wellbore is stimulated to κ = 100mDarcy over 3m radii. Well-core-centric permeability stimulation increases flow and/or lowers operating pressures to achieve more efficient heat transport within an EGS advection section.

On a bigger advective scale, Figure 8 compares conduction with advection for a wellbore-centric advective heat exchanger. For the conductive heat flow simulation (left), the central well extracts heat by passing fluid along the wellbore to cool the section to100^{o}C; no fluids flow in annular quartet of wellbores. For the advective heat flow simulation (right), fluid flows into the crustal section via the central wellbore and out of the section via the annular quartet of wellbores; the central wellbore fixed at 100^{o}C represents heat-depleted fluid injected into the heat exchange volume. For both conduction and advection, the heat exchanger outer boundary fixed at 200^{o}C conductively supplies heat from the ambient crust. In the absence of significant advection, thermal conduction results in a temperature distribution from 100^{o}C at the center to 200°C at the periphery, with Figure 9 (left) showing residual advective heat flux as blue arrows undeflected by the outtake wells. In the presence of significant fluid flow from the central wellbore, the advected fluid absorbs heat in the heat exchanger and transports the heat to the outtake wellbore as shown by the deflected blue arrows (Figure 9 right).

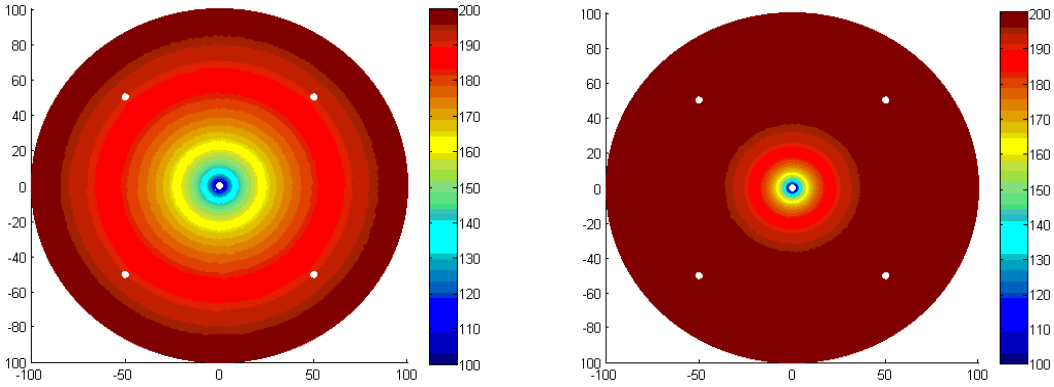

Figure 8 – (Left) Low advection rate = conductive steady-state temperature field determined by central extraction wellbore temperature 100°C for heat-exchange volume outer radius 100m at temperature 200°C; the temperature at 70m annular radius is 180°C. (Right) Equilibrium advection rate for fluid entering heat exchange volume from central wellbore at 100°C and moving radially towards the outtake wells; heat picked up by the advecting fluid in the heat exchange volume raises the temperature at the 70m outtake-well annular radius to 200°C.

The Figure 8 steady-state conductive regime with negligible advective flow distributes heat at 180°C at 70m radius, while delivering heat to the wellbore fluid at 100°C. By contrast, the rate of advective flow matching the conductive recharge across the advection heat exchanger delivers heat at 200°C at the annular outtake wellbore 70m radius with likelihood that the annular radius of outtake wellbores could be considerably reduced towards 35m.

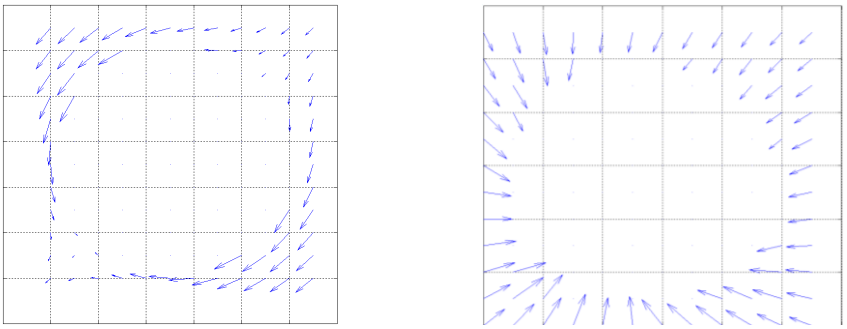

Fig 9 -- Left: Low advection rate = conductive steady-state heat flux at outtake wellbores determined by central extraction wellbore temperature 100°C and heat-exchange volume outer radius temperature 200°C. Right: Equilibrium advection rate with fluid entering heat exchange volume from central wellbore at 100°C moving radially towards outtake wells; heat picked up by the advecting fluid in the heat exchange volume raises the temperature at the outtake wells to 200°C.

4. SUMMARY/CONCLUSIONS

In accompanying Paper I (Leary et al 2015), we note that (i) by far the greatest success in extracting heat from the crust involves natural advection systems rather than conduction systems and (ii) elementary considerations show that conditioning EGS conduction heat volumes for base-load power provision, particularly as abstracted in Figure 1, requires unfeasibly many square-kilometers of intervention surface area. Accordingly, we have considered here means by which advection can be built into EGS projects focused on physical scales in line with direct-use heat rather than base-load heat extraction rates. This logic leads naturally to wellbore-centric EGS flow geometries in which borehole length (notionally horizontal) is a major degree of design freedom in supplying desired heat loads. Wellbore-centric EGS flow allows us to focus on advection-system permeability stimulation in radial

crustal sections in which we can adequately realise the complex heterogeneity of *in situ* flow properties reviewed in accompanying Paper II (Malin et al 2015).

In view of the physical complexity of *in situ* permeability, we have taken the conservative tactic of simulating permeability enhancement in wellbore-centric radial sections a few meters in radius, and showing how enhanced permeability in such annular volumes acts to reduce conductive heat flow loss due to strong thermal gradients near wellbores. We suggest that the relatively modest goal of enhancing permeability in wellbore-annular volumes is appropriate to the enormity of the 'EGS problem': making purely conductive heat resource volumes produce useful amounts of heat at rates competitive with fossil-fueled and nuclear power production means.

Figure 10, excerpted from Paper I, summarises the importance of EGS substituting advective thermal flow for conductive thermal flow at what might be called 'realistic production scales'. Each diagram represents the temperature field for a wellbore-centric crustal section of 100m radius held at an ambient crustal temperature ~300°C. At the left, heat is extracted at heat flow rate j ~1W/m^2 from the central wellbore as minimally required for commercial heat energy extraction; extraction rate j ~1W/m^2 cools the crustal rock to 50°C if heat is conductively transported from the crustal section periphery at 300°C (the auxiliary quartet of wellbores in the diagram is not used for pure conduction). Clearly 50°C heat recovery is non-commercial. The center diagram illustrates fictional heat extraction for a 35m radius wellbore, at which radius heat from periphery conductively reaches the wellbore at commercial temperature level ~200^{o}C. This diagram illustrates the importance of minimizing heat loss at high thermal gradients. The right-hand diagram shows an advective solution to the EGS thermal conductivity problem: the auxiliary quartet of wellbores can used to advect heat from the central wellbore for exit at the auxiliary wellbores at a commercial temperature ~200^{o}C. Figure 10 thus sets a template for, first, actively substituting advective flow for conductive flow in the vicinity of wellbores, and, second, establishing the scales of advection-aided heat extraction needed for commercial outcomes. We suggest that at some point, advective heat flow of scales of 10s of meters will have to be achieved in standard high temperature crustal rock. Much past experience further suggests this goal will be achieved only if we learn to master the art of *in situ* bulk permeability stimulation in the context of the wellbore-centric heat advective flows on m-Dm scales as modeled in Figures 7-10.

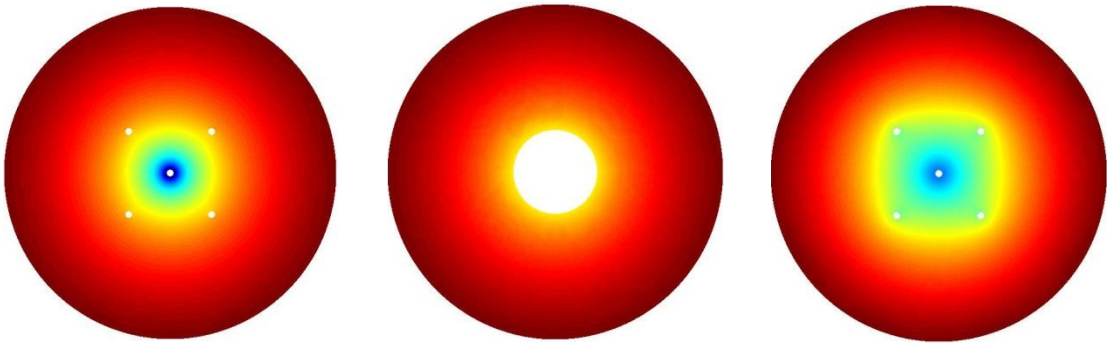

Figure 10. Diagrams representing the temperature field for a wellbore-centric crustal section of 100m radius held at 300°C. (Left) Heat is extracted at heat flow rate j ~1W/m^2 from the central wellbore (minimal requirement for commercial heat energy extraction); extraction rate j ~1W/m^2 cools the crustal rock to 50°C if heat is conductively transported from the crustal section periphery at 300°C (auxiliary quartet of wellbores not used for pure conduction). (Center) Heat extraction at fictional 35m radius wellbore; heat conducted from periphery reaches the wellbore at commercial temperature level ~200°C. (Right) Advective solution to the left-center EGS problem uses auxiliary quartet of wellbores to extract heat using fluid flow from the central wellbore; advective heat flow brings commercial grade temperatures ~200°C to the quartet of advective outtake wellbores.

REFERENCES

Ahrens LH (1963) Lognormal-type distributions in igneous rocks – IV, *Geochmica Cosmochim Acta* 27, 333-343.

Armstead HCH & Tester JW (1987) *Heat Mining*, E & FN Spon Ltd., NY.

Baghbanan A & Jing L (2008) Stress effects on permeability in a fractured rock mass with correlated fracture length and aperture, *International Journal of Rock Mechanics and Mining Sciences* 45, 1320-1334.

Bandis S (1980) Experimental studies of scale effects on shear strength and deformation of rock joints, PhD Thesis, Department of Earth Sciences, University of Leeds, pp540.

Biot MA (1941) General theory of three-dimensional consolidation, *Journal of Applied Physics* 12, 155-164.

Bodvarsson G (1969) On the temperature of water flowing through fractures, *J. Geophys. Res*. 74, 1987-1992.

Brace WF (1980) Permeability of crystalline and argillaceous rocks, *International Journal of Rock Mechanics, Mineral Science. & Geomechanics Abstracts* 17, 241-251.

Carslaw HS & Jaeger JC (1959) *Conduction of Heat in Solids*, Oxford University Press, pp510.

Clauser C (1992) Permeability of crystalline rocks, *EOS Transactions AGU* 73 No 21, 233-237.

Dahlen FA (1990) Critical taper model of fold-and-thrust belts and accretionary wedges, *Annual Reviews Earth Planet. Sci.* 18, 55-99.

Dahlen FA, Suppe J & Davis D (1984) Mechanics of fold-and-thrust belts and accretionary wedges' cohesive coulomb theory, *Journal of Geophysical Research* 89, 10,087-10,101

Davis D, Suppe J & Dahlen FA (1983) Mechanics of fold-and-thrust belts and accretionary wedges, *Journal of Geophysical Research* 88, 1153–1178.

Dunnicliff J (1993) *Geotechnical Instrumentation for Monitoring Field Performance*, J Wiley & Sons, pp608.

Earlougher RC (1977) *Advances in Well Test Analysis*, Society of Petroleum Engineers, Dallas, pp264.

Elsworth D (1989) Theory of thermal recovery from a spherically stimulated HDR reservoir, *J. Geophys. Res*. 94, 927-934.

Elsworth D (1990) A comparative evaluation of the parallel flow and spherical reservoir models of HDR geothermal systems, *J. Volcanology and Geothermal Res*. 44, 283-293.

Engelder T & Geiser P (1980) On the use of regional joint sets as trajectories of paleostress fields during the development of the Appalachian Plateau, New York, *J Geophys Res* 85, 6319-6341.

Freeze RA (1975), A Stochastic-Conceptual Analysis of One-dimensional Groundwater Flow in Non-uniform Homogeneous Media, *Water Resources Research*, 11, 725-741.

Geiser PA & Sansone S (1981) Joints, microfractures, and the formation of solution cleavage in limestone, *Geology* 9, 280-285.

Gelhar LW (1986) Stochastic subsurface hydrology from theory to applications, *Water Resource Research* 22, 135S-145S.

Gelhar LW, Welty C & Rehfeldt KR (1992) A critical review of data on field-scale dispersion in aquifers, *Water Resources Research* 28, 1955-1974.

Geller RJ, Jackson CC, Kagan YY & Mulargia F (1997) Earthquakes Cannot Be Predicted, *Science* 275, 1616.

Grindley GW (1965) The geology, structure and exploitation of the Wairakei geothermal field, Taupo, New Zealand, *N.Z. Geological Survey Bulletin* 75, 131.

Gringarten AC & Witherspoon PA (1973) Extraction of Heat from Multiple-Fractured Dry Hot Rock, *Geothermics* 2, No. 3-4, 119-122.

Gringarten AC, Witherspoon PA & Ohnishi Y (1975) Theory of heat extraction from fractured hot dry rock, *Journal of Geophysical Research* 80, 1120-1124.

Gutenberg B & Richter CF (1956) Earthquake Magnitude, Intensity, Energy, and Acceleration (Second Paper), *Seismological Society of America Bulletin* 46, 105-145.

Hanano M (2000) Two different roles of fractures in geothermal development, *Proceedings World Geothermal Congress* 2000, Kyushu - Tohoku, Japan, May28-June10 2000.

Hanks TC & Kanamori H (1979) A moment magnitude scale, *J. Geophys. Res*. 84, 2348–2351.

Heuer N, Kupper T & Windelberg D (1991) Mathematical model of a hot dry rock system, *Geophys. J. Int.* 105, 659-664.

Hirata T (1989) Fractal dimension of fault systems in Japan: Fractal structure in rock fracture geometry at various scales, *Pure Appl. Geophys*. 131, 157– 170.

Hirata T, Satoh T & Ito K (1987) Fractal structure of spatial distribution of microfracturing in rock, *Geophys. J. R. astr. Soc.* 90.

Horne RN (1995) *Modern Well Test Analysis*, Petroway Inc, ISBN 0-9626992-1-7, pp257.

Horner DR (1951) Pressure build-up in wells, In: Third World Petroleum Congress, The Hague, pp 503-523; also Pressure Analysis Methods, SPE Preprint Series 9, pp 25-43, 1967.

Howard, GC & Fast CR (1970) Hydraulic fracturing, *Society of Petroleum Engineers of AIME*, pp203.

Hubbert MK & Rubey WW (1959) Role of fluid pressure in mechanics of overthrust faulting, *Bulletin Geological Society of America* 70, 115-166.

Hubbert MK & Willis DG (1957) Mechanics of Hydraulic Fracturing, *Transactions of Society of Petroleum Engineers of AIME* 210, 153-168.

Jaeger JC & Cook NGW (1979) *Fundamentals of Rock Mechanics*, Chapman and Hall, pp593

Jensen JL, Lake LW, Corbett PWM & Goggin D (1997) Statistics for Petroleum Engineers and Geoscientists, Prentice-Hall, NJ, pp390.

Juliusson E (2012) Characterization of fractured geothermal reservoirs based on production data, Stanford Geothermal Program, Stanford University, Stanford, CA

Kagan YY & Knopoff L (1980) Spatial distribution of earthquakes: the two-point correlation function, *Geophys. J. R. astr. Soc.* 62, 303-320.

King G (1983) The accommodation of large strains in the upper lithosphere of the Earth and other solids by self-similar fault systems: The geometrical origin of b-value, *Pure Appl. Geophys.* 121, 761– 815.

Kitanidis PK (1997) *Introduction to Geostatistics*, Cambridge University Press, pp249.

Koch GS & Link RF (1971) The coefficient of variation; a guide to the sampling of ore deposits, *Economic Geology* 66, 293-301.

Law J (1944) A statistical approach to the interstitial heterogeneity of sand reservoirs, Technical Publication 1732, *Petroleum Technology* 7, May 1944.

Leary P, Malin P, Geiser P, Pogacnik J, Rugis J & Valles B (2015) Flow Lognormality & Spatial Correlation in Crustal Reservoirs – I: Physical Character & Consequences for Geothermal Energy, WGC2015, 19-24 April 2015, Melbourne AU.

Leary P, Malin P, Pogacnik J, Rugis J, Valles B & Geiser P (2014) Lognormality, $\delta\kappa \sim \kappa\, \delta\varphi$, EGS, and All That, *Proceedings 39th Stanford Geothermal Workshop*, Stanford University.

Leary P, Pogacnik J & Malin (2013) Prospects for Enhanced Single-Well Heat Extraction, *Proceedings 35th New Zealand Geothermal Worksho*p, Rotorua.

Leary P, Pogacnik J & Malin P (2012) Computational EGS -- Heat transport in 1/*f*-noise fractured media, *Proceedings 37th Stanford Geothermal Workshop*, Stanford University.

Leary PC (2002a) Fractures and physical heterogeneity in crustal rock, in *Heterogeneity of the Crust and Upper Mantle – Nature, Scaling and Seismic Properties*, J. A. Goff, & K. Holliger (eds.), Kluwer Academic/Plenum Publishers, New York, 155-186.

Leary PC (2002b) Numerical simulation of first-order backscattered P and S waves for time-lapse seismic imaging in heterogeneous reservoirs, *Geophysical Journal International* 148, 402–425.

Leary PC & Al-Kindy F (2002) Power-law scaling of spatially correlated porosity and log(permeability) sequences from north-central North Sea Brae oilfield well core, *Geophysical Journal International* 148, 426-442.

Leary PC (1997) Rock as a critical-point system and the inherent implausibility of reliable earthquake prediction, *Geophysical Journal International* 131, 451-466.

Leary P & Abercrombie RE (1994a) Frequency dependent crustal scattering and absorption at 5-160 Hz from coda decay observed at 2.5 km depth, *Geophysical Research Letters* **21**, 971-974.

Leary P & Abercrombie RE (1994b) Fractal fracture scattering origin of S-wave coda: spectral evidence from recordings at 2.5 km, *Geophysical Research Letters* **21**, 1683-1686.

Leary PC (1991) Deep borehole log evidence for fractal distribution of fractures in crystalline rock, *Geophysical Journal International* 107, 615-628.

Limpert E, Stahel W & Abbt M (2001) Log-normal Distributions across the Sciences: Keys and Clues, *BioScience* 51, 341–352.

Malin P, Leary P, Shalev E, Rugis J, Valles B, Boese C, Andrews J & Geiser P (2015) Flow Lognormality and Spatial Correlation in Crustal Reservoirs: II – Where-to-Drill Guidance via Acoustic/Seismic Imaging, WGC2015, 19-24 April 2015, Melbourne AU.

Mavko G, Mukerji T & Dvorkin J (2003) *The Rock Physics Handbook: Tools for Seismic Analysis in Porous Media*, Cambridge University Press, pp329;

Mesri G & Olson R (1971) Mechanisms controlling the permeability of clays, *Clays and Clay Minerals* 19, 151-158.

Molnar P, Anderson RS & Anderson SP (2007) Tectonics, fracturing of rock, and erosion, *Journal of Geophysical Research* 112, F03014-03026.

Muskat M (1937) *The Flow of Homogeneous Fluids Through Porous Media*, McGraw-Hill, pp763.

Neuman SP (1994) Generalized scaling of permeabilities: Validation and effect of support scale, *Geophys. Res. Lett*. 21, 349–352.

Neuman SP (1995) On advective dispersion in fractal velocity and permeability fields, *Water Resources Research* 31, 1455–1460.

Petty S (2013) Newberry EGS Demonstration, *DOE Geothermal Technologies Office Peer Review*, April 22, 2013

Pogacnik J, Leary P, Malin P, Geiser P, Rugis R & Valles B (2015) Flow Lognormality and Spatial Correlation in Crustal Reservoirs: III -- Natural Permeability Enhancement via Biot Fluid-Rock Coupling At All Scales, WGC2015, 19-24 April 2015, Melbourne AU.

Pogacnik J, Leary P & Malin P (2013) CGS – Controlled wellbore-to-wellbore geothermal system flow, *Proceedings 38th Stanford Geothermal Workshop*, Stanford University.

Pruess K & Narasimhan TN (1985) A practical method for modeling fluid and heat flow in fractured porous media, *Society of Petroleum Engineers Journal*, SPE10509, 14-26.

Pusch R , Weston R & Knutsson S (2014) Impact of scale on rock strength, *Journal of Earth Sciences and Geotechnical Engineering* (in press)

Reid PW, Messeiller M, Llanos EM & Hasting M (2011) Paralana 2 – Well Testing and Stimulation, *Proceedings Australian Geothermal Energy Conference*, Melbourne.

Schulze-Makuck D & Cherhauer DS (1995) Relation of hydraulic conductivity and dispersivity to scale of measurement in a carbonate aquifer, In: *Models for Assessing and Monitoring Groundwater Quality*, ed. By B.J. Wagner, T. H. Illangasekare & K. H. Jensen, IAHA Publication No. 227.

Simpson DW & Negmatullaev SK (1980) Induced seismicity at Nurek Reservoir, Tadjikistan, USSR, *Bulletin of the Seismological Society of America* 70, 1561-1586

Simpson DW, Leith WS & Scholz CH (1988) Two types of reservoir-induced seismicity, *Bulletin of the Seismological Society of America* 78, 2025-2040.

Sutter D, Fox DB, Anderson BJ, Koch DL, von Rohr PR &Tester JW (2011) Sustainable heat farming of geothermal systems: a case study of heat extraction and thermal recovery in a model EGS fractured reservoir, *Proceedings 36th Workshop on Geothermal Reservoir Engineering*, Stanford University, January 31-February 2.

Tavernas F, Jean P, Leblond P, & Leroueil S (1983) The permeability of natural soft clays, Part II: Permeability Characteristics, *Canadian Geotechnical Journal* 21, 6.

Taylor DW (1948) *Fundamentals of Soil Mechanics*, New York, J Wiley & Sons, 345.

Terzaghi K (1925) *Erdbaumechanik*, Franz Deuticke, Vienna, Austria.

Tester JW et al. (2006), *The Future of Geothermal Energy -- Impact of Enhanced Geothermal Systems (EGS) on the United States in the 21st Century*, Massachusetts Institute of Technology, pp372. http://geothermal.inel.gov; http://www1.eere.energy.gov/geothermal/egs_technology.html

Theis CV (1935) *Transactions of the American Geophysical Union*, Part 2, 519-524, August 1935; also Theis CV (1952) The relation between lowering of the piezometric surface and the rate and duration of discharge of a well using ground water storage, Ground Water Notes No 5, Hydraulics, United States Geological Survey, Water Resources Division, Ground Water Branch.

Winter CL & Tartakovsky DM (2001) Theoretical Foundation for Conductivity Scaling, *Geophysical Research Letters* 22, 4367-4369.

Wunder R & Murphy H (1978) Thermal drawdown and recovery of singly and multiply fracture hot dry reservoirs, Report LA-7219-MS, Los Alamos National Laboratory, 15pp.

Zikovsky L & Chah B (1990) The lognormal distribution of radon concentration in ground water, *Ground Water* 28, No. 5, 673-676.